Preparation and Characterizations of Tantalum Pentoxide (Ta_2O_5) Nanoparticles and UV-Curable Ta_2O_5-Acrylic Nanocomposites

Heh-Chang Huang, Tsung-Eong Hsieh

Department of Materials Science and Engineering, National Chiao Tung University, Hsinchu, Taiwan 30010, Republic of China

Received 13 October 2008; accepted 26 October 2009
DOI 10.1002/app.31709
Published online 26 March 2010 in Wiley InterScience (www.interscience.wiley.com).

ABSTRACT: Tantalum pentoxide (Ta_2O_5) nanoparticles with the sizes in the range of 20–50 nm were prepared via a chemical route in which the oleic acid (OLEA) was adopted as the surfactant for the synthesis process. X-ray diffraction (XRD) revealed the as-synthesized Ta_2O_5 transforms from amorphous to hexagonal and orthorhombic structures at the temperatures of 700°C and 750°C, respectively, illustrating the suppression of recrystallization temperature of Ta_2O_5 due to the particle size reduction. UV-curable nanocomposites containing the Ta_2O_5 nanoparticles and acrylic matrix were also prepared. Thermogravimetry analysis (TGA) found an about 10–20°C improvement on the 5% weight-loss thermal decomposition temperatures (T_ds). Dielectric measurement showed that the dielectric constant of nanocomposite increases with the increase in the filler loading without severe deterioration of dielectric loss. The increment of dielectric constants was ascribed to the addition of high-dielectric inorganic fillers as well as the presence of interfacial polarization at the organic/inorganic interfaces. © 2010 Wiley Periodicals, Inc. J Appl Polym Sci 117: 1252–1259, 2010

Key words: dielectric properties; nanocomposites; tantalum pentoxide; acrylic polymer; UV-curable nanocomposites; dielectric properties

INTRODUCTION

Recently, numerous efforts have been poured into the research and development of flexible electronic devices due to the pursuit of inexpensive, compact, and light-weight electronic products with good portability.[1,2] However, in addition to the mechanical flexibility, the materials for flexible electronics must be compatible to low-temperature and large-area fabrication processes due to the production demands for flexible substrates. One of the promising candidates would be the UV-curable polymeric and/or composite materials with satisfactory physical/chemical properties.

In the fabrication of semiconductor devices, high dielectric constant materials are essential part for gate insulators of devices. In conventional integrated circuit (IC) fabrications, silicon dioxide (SiO_2) with relative dielectric constant (κ) $\sim$ 3.9 or silicon nitride (Si_3N_4) with $\kappa \sim 7.9$ is widely adopted for relative applications. High-κ polymers are similarly required for the fabrication of flexible electronics; nevertheless, it is difficult for sole polymeric materials to meet such a requirement because they rarely possess the values of $\kappa > 4$. A common way to manipulate the dielectric properties is to form the composite by incorporating the inorganic filler with high-κ property in polymeric matrix. Formation of composites also leads to the improvement of physical properties such as, thermal, mechanical, and permeation properties to meet the device processing and reliability requirements. At present, the addition of high dielectric permittivity ceramic powders, such as, zinc oxide (ZnO, $\kappa \sim 9$),[3] alumina (Al_2O_3, $\kappa \sim 9.8$),[4] and titanium oxide (TiO_2, $\kappa \sim 31$)[5,6] in the polymeric matrix have been reported. Hong et al. reported 20% increase of κ for ZnO nanoparticles-polyethylene (PE) composites.[3] The Al_2O_3-polyimide (PI) composites exhibited the value of $\kappa \sim 30$,[4] whereas a three-time improvement on the value of κ was achieved in nano-scale TiO_2-polystyrene (PS) composites.[6] In theoretical side, dielectric properties of binary phase composites have been widely studied in terms of the well-known mixing rules, such as, Maxwell-Garnett effective medium approximations[7]:

$$\varepsilon_{\text{com}} = \varepsilon_m \frac{\varepsilon_f + 2\varepsilon_m + 2f(\varepsilon_f - \varepsilon_m)}{\varepsilon_f + 2\varepsilon_m - f(\varepsilon_f - \varepsilon_m)}, \quad (1)$$

Correspondence to: T.-E. Hsieh (tehsieh@mail.nctu.edu.tw).

Contract grant sponsor: National Science Council (NSC), Taiwan, R.O.C.; contract grant number: NSC95-2221-E009–130.

where ε_{com} is dielectric constant of composites, ε_m is dielectric constant of matrix phase, ε_f is dielectric constant of filler, and f is the volume fraction of filler. The Maxwell-Garnett formula is derived based on homogeneous composites containing spherical filler particles. Nevertheless, because the interactions in between the filler and matrix phase are ignored during the derivation, the measured dielectric constants of composites usually deviate from the values predicted by Maxwell-Garnett formula due to the presence of chemical coupling agent effects,[3,8] interactions between organic and inorganic phases,[6,9] interfacial polarization,[4,10–14] etc. Another approach to modify the dielectric constants of polymer-based composites is to add the conductive fillers, such as, silver (Ag),[15] carbon nanotube (CNT),[16] nickel (Ni),[17] and aluminum (Al)[18] in polymeric matrices. The values of $\kappa \sim 300$, 1200, and 400 have been reported for Ag-epoxy,[15] CNT-rubber,[16] and Ni-polyvinylidene fluoride (PVDF)[17] composites, respectively. According to the percolation model,[16–18] the dielectric constant of nanocomposites containing conductive fillers would reach a limiting value when the filler content approaches to percolation threshold.[15,16] Nevertheless, it usually accompanies with a severe dielectric loss due to the filler aggregation in such composite systems. Furthermore, reduction of total surface energy would ignite aggregation in the samples containing nano-scale particles. A uniform dispersion of inorganic fillers is thus the key issue for the preparation of organic-inorganic composites, when the filler sizes approach nanometer scale. Modification of nano-scale particles so as to change their surface polarity is generally adopted to promote their dispersion in polymer matrix.[6]

Tantalum pentoxide (Ta_2O_5) is a well-known dielectric material for its relatively high dielectric constant ($\sim$ 24),[19] low leakage current density ($<10^{-7}$ A/cm^2 at the applied field 3 MV/cm), and high dielectric breakdown strength (>1 MV/cm).[20] However, there is no study relating to the Ta_2O_5-polymer composites, in particular, the UV-curable Ta_2O_5-polymer nanocomposite that is feasible to the fabrication of flexible electronics. This work reports a chemical route to synthesize the Ta_2O_5 nanoparticles with various crystallinities via the control of annealing temperatures. During the preparation of Ta_2O_5 nanoparticles, oleic acid (OLEA) was adopted as the surfactant as well as the solvent due to its low cost and the ease of chelating with metal and removal from particle surface afterward.[21,22] The nano-scale Ta_2O_5 particles were subsequently implanted in the UV-curable acrylic resin to form the nanocomposites and the characterizations of their microstructure and thermal/dielectric properties are presented as follows.

EXPERIMENTAL

Materials

Tantalum ethoxide with purity = 99.99% was purchased from Strem and OLEA was purchased from SHOWA. Ethanol (purity = 99.5%) and methyl methacrylate (MMA, purity = 99%) were purchased from Fluka. 2-Hydroxyethyl methacrylate (HEMA, purity = 98%) and Ta_2O_5 (purity = 99.99%, particle sizes = 0.1–0.5 μm) were purchased from Acros. Trimethylolpropane triacrylate (TMPTA, purity = 98%) and photoinitiator (chemcure 481) was purchased from Chembridge. All reagents were used without further purification.

Synthesis of Ta_2O_5 nanoparticles

First, the OLEA (35 g) was degassed in vacuum at 120°C for 1 h. Tantalum ethoxide (1.2 mL) was then injected into the OLEA solution and the reaction was carried out at 120°C for 1.5 h in Ar ambient. Afterward, DI water (0.2 mL) was added to the above solution and the reaction was further allowed for 24–48 h at 120°C in Ar ambient. After adding the ethanol, the Ta_2O_5 precipitates were obtained and they were dried in vacuum at room temperature. Subsequently, the Ta_2O_5 was sintered at 700°C or 750°C at a heating rate = 25°C/min for various time spans in air to yield the Ta_2O_5 nanoparticles. Formation of Ta—O—Ta network is achieved via hydrolysis and polycondensation processes.[21,23] As illustrated in eq. (2), hydrolysis results in the unstable hydroxyalkoxides, $Ta(OH)_x(OR)_{5-x}$. The polycondensation depicted by eq. (3) then leads to the Ta—O—Ta network via olation or oxolation reaction. The OLEA provided the micelle structure and limited further growth of Ta_2O_5 nanoparticles.[20]

$$Ta(OR)_5 + xH_2O \rightarrow Ta(OH)_x(OR)_{5-x} + xROH \quad (2)$$

$$(OR)_{5-x}(OH)_{x-1}Ta\text{–}OH + XO\text{–}Ta(OH)_x(OR)_{4-x} \rightarrow (OR)_{5-x}(OH)_{x-1}Ta\text{–}O\text{–}Ta(OR)_{4-x}(OH)_x + XOH \quad (3)$$

where $R = -C_2H_5$; X = H, R.

Preparation of UV-curable Ta_2O_5-acrylic nanocomposites

First, the as-synthesized Ta_2O_5 powder was heat-treated at 750°C for 9 h to yield the orthorhombic Ta_2O_5. Various amounts of Ta_2O_5 powders were then blended with MMA (1.5018 g; 0.015 mol), HEMA (1.17126 g; 0.009 mol), TMPTA (1.77792 g; 0.006 mol), and chemcure 481 photoinitiator (0.18546

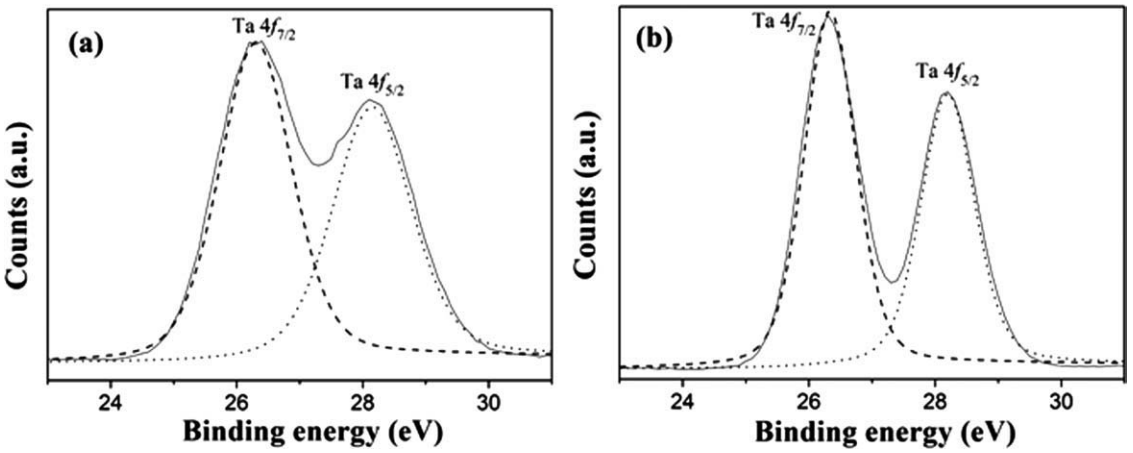

Figure 1 XPS spectra and curve fitting results for (a) as-synthesized Ta_2O_5 and (b) Ta_2O_5 annealed at 750°C for 9 h.

g; 4 wt %) in ethanol (2 mL). The mixtures were stirred at room temperature for 24 h in Ar ambient. The ethanol was then removed by reduced pressure distillation to form the Ta_2O_5-acrylic nanocomposite precursor. The nanocomposite precursor was coated on a polyester (PET) mold and cured by UV irradiation to obtain the nanocomposite thin-film samples with thickness about 300 μm. The photo-polymerization was carried out in an UV oven (C-SUN CU1000, Taiwan) with principal wavelength = 365 nm, curing power = 80 W/cm, and curing time = 50 to 90 s.

For comparison purpose, the orthorhombic Ta_2O_5 raw powder with sizes in the range of 0.1–0.5 μm was also adopted to prepare the UV-curable Ta_2O_5-acrylic composite. In this work, the thin-film composite containing 4 wt % of Ta_2O_5 was prepared according to the procedures described earlier.

Structure and property characterizations

X-ray photoelectron spectroscopy (XPS, American Physical Electronics ESCA PHI 1600) was adopted to analyze the bonding status of Ta_2O_5 powders by using an Mg-K_α source. Crystal structures of synthesized Ta_2O_5 powders were characterized by an X-ray diffractrometer (XRD, MacScience M18XHF) within Cu-K_α radiation ($\lambda = 0.154$ nm) at a scan rate of 2°/min. Thermogravimetric analysis/derivative thermogravimetry analysis (TGA/DTA) spectra were recorded by a Mettler-Toledo tga/sdta851 TGA operating in air atmosphere at a heating rate = 10°C/min. Surface morphologies of Ta_2O_5 powders were characterized by a field-emission scanning electron microscope (FE-SEM, Hitachi S4700). Microstructure of Ta_2O_5-acrylic nanocomposite was examined by transmission electron microscopy (TEM, JEOL JEM-2100) with operating voltage = 200 kV to reveal the distribution of Ta_2O_5 nanoparticles in polymeric matrix. Chemical structure of Ta_2O_5-acrylic nanocomposite was characterized by Fourier transform infrared spectrometer (FTIR, PerkinElmer spectrum 100). The metal–insulator-metal (MIM) samples with UV-cured Ta_2O_5-acrylic nanocomposite as the insulator layer were prepared for dielectric measurement. The top and bottom electrodes were Ag layers prepared by screen printing of Ag paste. After drying in vacuum for at least 24 h, the capacitances of MIM samples were measured by an HP 4194A gain/impedance analyzer operating in the frequency range of 1–10 MHz and an HP 4291B impedance analyzer operating in the frequency range of 10–600 MHz, respectively. The relative dielectric constant κ was calculated according to the formula as follows:

$$\kappa = \frac{Ct}{\varepsilon_o A}, \tag{4}$$

where C = capacitance, ε_o = the vacuum dielectric permittivity, A = the area of electrode = 0.283 cm^2, and t = the thickness of cured nanocomposite layer = 300 μm. The MIM samples were also transferred to an HP 4156B semiconductor parameter analyzer for the measurement of leakage current densities of samples.

RESULTS AND DISCUSSION

Synthesis, annealing, and microstructure of Ta_2O_5 nanoparticles

XPS was carried out to characterize the bonding status of synthesized products. The curve fittings were achieved by using the XPSPEAK 4.1 program with a combination of Gaussian (80%) and Lorentzian (20%) distributions. The oxidation state of as-synthesized Ta_2O_5 and the Ta_2O_5 sintered at 750°C for 9 h are shown in Figure 1(a,b), respectively. In both XPS spectra, the Ta $4f_{7/2}$ and Ta $4f_{5/2}$ with binding

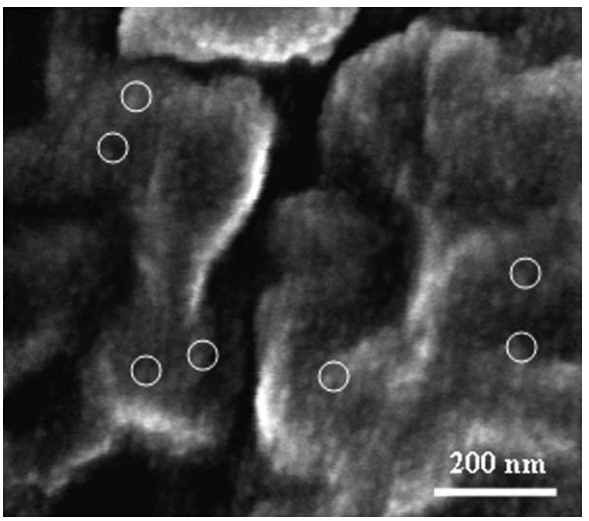

Figure 2 SEM image of as-synthesized Ta_2O_5. Nano-scale Ta_2O_5 particles (several of them are highlighted by open circles) aggregate into granules due to the lack of dispersion.

energies at 26.3 and 28.2 eV are observed, confirming the synthesized products are indeed Ta_2O_5.[24]

Figure 2 shows the SEM micrograph of as-synthesized Ta_2O_5 in which the granules comprised of the aggregation of Ta_2O_5 particles with sizes about 20–25 nm can be seen. The size confinement of Ta_2O_5 particles is ascribed to the complex formed by the reactions of OLEA and tantalum ethoxide during the synthesis. However, due to the absence of dispersion treatment at this step, the nano-scale Ta_2O_5 particles aggregate in order to reduce the total surface energy so that relatively large Ta_2O_5 granules with sizes about several hundred nanometers present in Figure 2. Furthermore, the XRD characterization shown in Figure 3 reveals that the as-synthesized Ta_2O_5 is essentially amorphous.

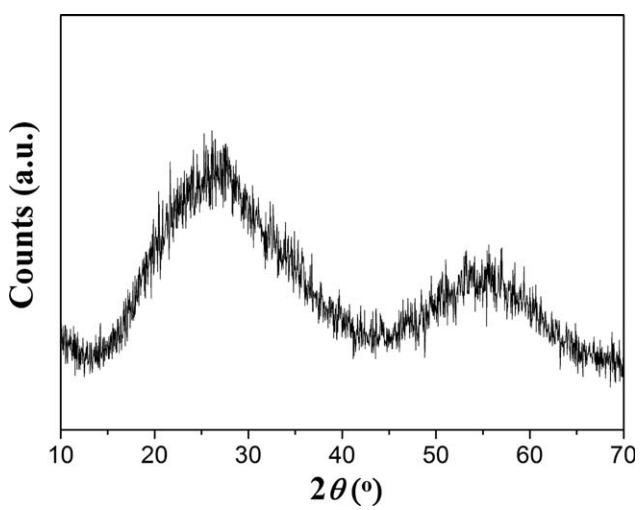

Figure 3 XRD pattern of as-synthesized Ta_2O_5.

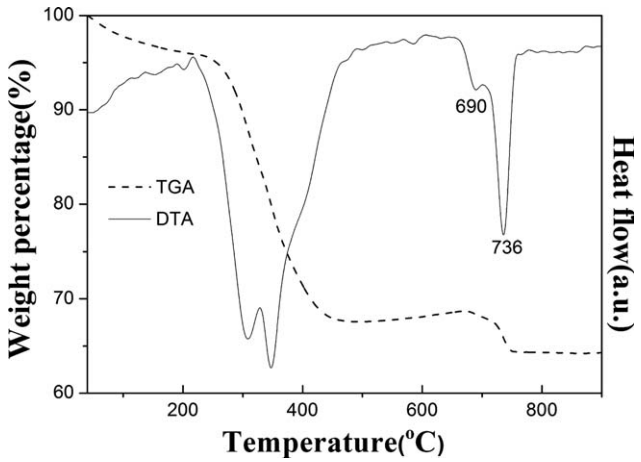

Figure 4 TGA/DTA diagram of as-synthesized Ta_2O_5.

The TGA/DTA diagram of as-synthesized Ta_2O_5 is presented in Figure 4. The TGA profile indicates that the organic components decompose at the temperatures ranging from 250°C to 400°C, whereas the phase changes of Ta_2O_5 occur in the temperatures ranging from 650°C to 750°C. As shown by the DTA curve in Figure 4, the phase changes of Ta_2O_5 sequentially occur at 690°C and 736°C. As a result, we performed the annealing treatments at 700°C and 750°C, respectively, and subsequently, sent the samples to XRD apparatus for phase structure identification.

As shown in Figure 5, the Ta_2O_5 annealed at 700°C for 9 h is hexagonal phase (JCPDS:19–1299) and then Ta_2O_5 transforms to orthorhombic phase (JCPDS:25–922) when the annealing temperature further rises to 750°C. The inset at right-hand corner of Figure 5 is the enlarged XRD pattern in the 2θ range of 40–55°. The phase transition is evidenced by the emergence of $(3,4,0)_{2\theta\ =\ 44.74^\circ}$ orthorhombic phase

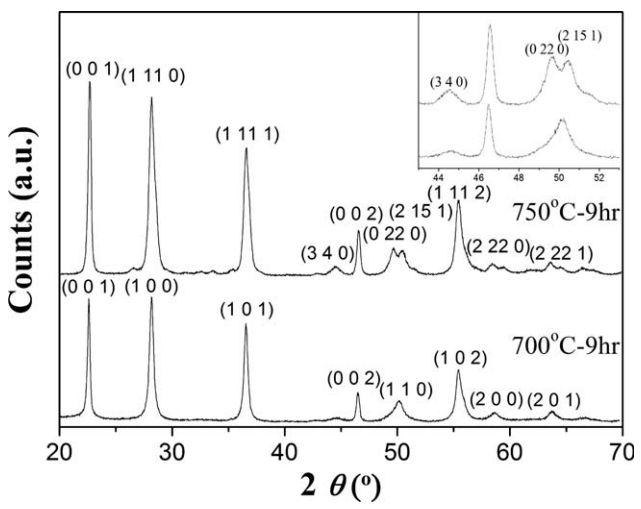

Figure 5 XRD patterns of Ta_2O_5 annealed at 700°C and 750°C for 3 h.

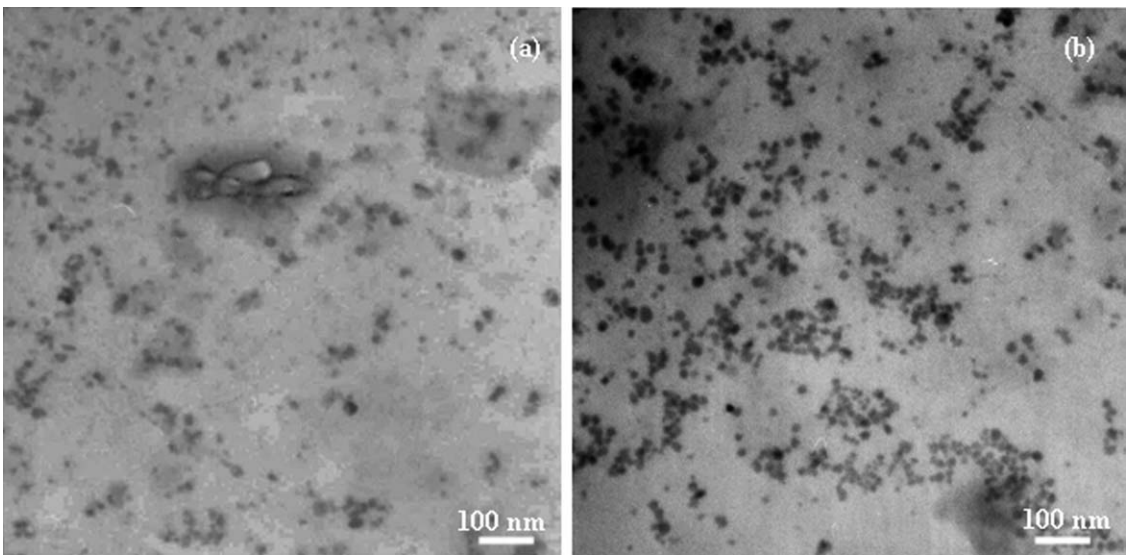

Figure 6 TEM images of nanocomposite samples containing (a) 3 wt % and (b) 10 wt % of Ta_2O_5. The filler particles were prepared via the annealing of as-synthesized Ta_2O_5 at 750°C for 9 h.

peak as well as the split of $(1,0,0)_{2\theta = 50.35^\circ}$ hexagonal phase peak into $(0,22,0)_{2\theta = 49.73^\circ}$ and $(2,15,1)_{2\theta = 50.7^\circ}$ orthorhombic phase peaks.[22] Because the particle size of orthorhombic Ta_2O_5 remains in nano-scale, it would result in the XRD peak broadening and cause partial overlap of (0,22,0) and (2,15,1) peaks.[25] We have eliminated the background noise during XRD analysis and the results above indeed reveal the hexagonal-to-orthorhombic transformation of Ta_2O_5 when annealing temperature is increased from 700°C to 750°C. It is known that, in general, the recrystallization temperature of orthorhombic Ta_2O_5 bulk phase is about 800–1000°C.[26–28] The results above illustrated that, by reducing the particle size to nanometer scale, the orthorhombic Ta_2O_5 phase could be obtained at a temperature below 750°C. The suppression of phase-transition temperature is believed to be driven by the presence of numerous interfaces resulted from the particle size reduction. The interfacial-driven effects allow an easy atomic rearrangement in Ta_2O_5 lattice, and thus ignite the phase change at lower temperatures.

We note that in this study the annealing treatment up to 750°C does not cause significant Ta_2O_5 particle coarsening. During the annealing process, OLEA might be burned to form porous char around Ta_2O_5 nanoparticles when the temperature reached 500°C and then the char serves as the barrier to the coalescence of Ta_2O_5 particles during high-temperature annealing at 750°C. Subsequent mechanical agitation and ultrasonic vibration of Ta_2O_5 nanoparticles would wash away the char in ethanol solution and break off the possible necking in between Ta_2O_5 nanoparticles induced in annealing process.

The Ta_2O_5 particle sizes were also calculated by plugging the XRD data presented in Figure 5 into Scherrer's equation.[25] The results, for instance, the particle size of Ta_2O_5 sample sintered at 750°C for 3 h is about 18 nm, are in good agreement with subsequent TEM observations shown in Figure 6.

Characterizations of Ta_2O_5-acrylic nanocomposites

Figure 6(a,b) shows the TEM images of cured nanocomposite sample containing 3 wt % and 10 wt % of Ta_2O_5, respectively. The filler particles were prepared via the annealing of as-synthesized Ta_2O_5 at 750°C for 9 h. The nano-scale Ta_2O_5 particles with the sizes about 20–25 nm embedded in acrylic matrix can be readily seen. Because the Ta_2O_5 possesses hydrophilic feature, we thus utilized the hydrophilic HEMA monomer (i.e., the monomer contains —OH functional group)[9,29] in conjunction with mechanical agitation and ultrasonic vibration to enhance the compatibility between organic and inorganic components in nanocomposites. This provides a fairly good dispersion of nano-scale Ta_2O_5 particles in polymeric matrix.

Table I lists the 5% weight-loss thermal decomposition temperatures (T_ds) and residual weights of Ta_2O_5-acrylic nanocomposites containing various amounts of Ta_2O_5 obtained by TGA analysis. In comparison with pristine acrylic, thermal stability of nanocomposites is clearly improved due to the addition of Ta_2O_5. However, in the samples with high filler loading, e.g., the samples containing 7 wt % and 10 wt % of Ta_2O_5, the T_ds decrease slightly. During the sample preparation, it was observed that the samples with high filler loading require longer curing times to complete the photo-polymerization. It is speculated that the too many Ta_2O_5 particles may hinder the propagation of UV light into the interior

TABLE I
T_ds and Residual Weights of Ta_2O_5-Acrylic Nanocomposites Obtained by TGA Analysis

Sample	Ta_2O_5 content (wt %)	T_d (°C)	Residual weight (wt %)
Pristine acrylic	0	313.0	–
Nanocomposite	3	322.5	3.37
	3.5	324.8	3.82
	4	329.1	4.34
	4.5	332.7	4.86
	7	330.8	7.58
	10	323.4	10.59

of nanocomposites and thus cause the incomplete sample curing. A prolonged curing time was thus required for high-filler-loading samples; nevertheless, excessive UV exposure might induce the photodegradation of polymer matrix and lead to the degradation of thermal stability of nanocomposite samples.[30–32]

Figure 7(a,b) separately present the dielectric constants and dielectric losses of nanocomposite samples containing various amounts of Ta_2O_5 measured in the frequency range of 1–600 MHz. We note the data discontinuities at 10 MHz were resulted from the difference of measuring frequency ranges of HP 4194A and HP 4291B. It can be readily seen that both the dielectric constant and dielectric loss of nanocomposite increase with the increase of Ta_2O_5 content. The nanocomposite sample containing 4.5 wt % Ta_2O_5, i.e., the sample with the highest thermal stability, exhibits an about 60% increment on the dielectric constant in comparison with the pristine acrylic over the measured frequency range. Figure 7(a) further shows that the increasing trend of dielectric constant gradually alleviates when the filler loading exceeds 4.5 wt %. This is mainly attributed to the aggregation of Ta_2O_5 nanoparticles in nanocomposites with high filler loading, and thus the reduction of interfacial polarization contributing to the dielectric property. We note that photo-degradation induced by the excessive UV curing may be another cause of the alleviation of dielectric constant increment in the nanocomposites with high filler loading.

Figure 7(b) shows that the nanocomposites exhibit a slightly higher dielectric loss in comparison with the pristine acrylic, implying that the addition of Ta_2O_5 nanoparticles causes no dramatic change on the loss mechanism. In the studies relating to high dielectric constant materials, it has been reported that electrical domain walls in $BaTiO_3$ gradually diminish when grain size is scaled down to submicro scale.[33] TEM characterization on lead zirconate titanate (PZT) films showed that the domain sizes in such a high-κ dielectric are about 10–15 nm.[34] In terms of the filler sizes revealed by TEM shown in Figure 6, it is speculated that the Ta_2O_5 nanoparticles may hence be approximate as individual electric dipoles (i.e., sole electrical domain in each of the Ta_2O_5 nanoparticles) with few of them contain domain walls. Furthermore, the Ta_2O_5 nanoparticles dispersed in polymeric matrix are separated by a distance of several tens nanometers, which is comparatively larger than that of the dipoles intimately aligned in the domains of large-grained dielectrics. A comparatively weak coupling between neighboring dipoles (i.e., the dispersed Ta_2O_5) in the nanocomposites can thus be expected because Coulomb's attraction is inversely proportional to the square of distance. When an alternative external bias at MHz frequency range is applied, it is would be easier for the weakly-coupled dipoles to switch along with the direction of bias field. In addition, few domain wall motions are involved during the dipole switching so that less electrical energy was consumed. No dramatic dielectric loss was hence observed in our Ta_2O_5-acrylic nanocomposites. Suppression of dielectric loss was similarly observed in the studies relating to nano-$BaTiO_3$ ceramics

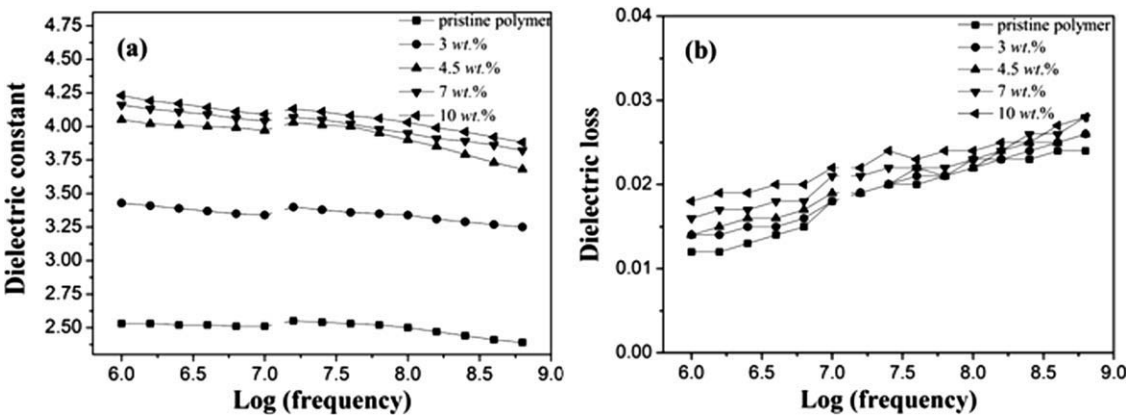

Figure 7 (a) Dielectric constant and (b) dielectric loss of Ta_2O_5-acrylic nanocomposites as a function of measurement frequency.

TABLE II
A List of Calculated and Measured Dielectric Constants of Nanocomposites

Sample	Ta_2O_5 content (wt %)	Calculated value[a]	Experimental value[b]
Pristine acrylic	0	2.53	2.53
Nanocomposite	3	2.56	3.43
	3.5	2.56	3.86
	4	2.56	3.98
	4.5	2.57	4.05
	7	2.59	4.16
	10	2.62	4.23
Composite[c]	4	2.56	3.25

[a] Dielectric constant of orthorhombic Ta_2O_5 phase (=24) was adopted for calculation.
[b] Experimental values were measured at 1 MHz.
[c] Sizes of Ta_2O_5 filler particles in composite sample range from 0.1 to 0.5 μm.

based on the assumption of individual electric dipole with relatively few domain wall motions as presented earlier.[35,36]

Table II lists the experimental values (measured at 1 MHz) and theoretical values of dielectric constants for nanocomposites calculated in terms of the Maxwell-Garnett approximation given by eq. (1). It can be readily seen that the measured values for nanocomposite samples are always higher than those obtained by calculation regardless of the Ta_2O_5 filler loading. For comparison, we also prepared a composite sample containing 4 wt % orthorhombic Ta_2O_5 particles with larger sizes in the range of 0.1–0.5 μm. It was found that the dielectric constant of the composite sample (= 3.25) is higher than the calculated value (= 2.56), but lower than that of the nanocomposite sample containing the same amount of nano-scale Ta_2O_5 (= 3.98). We ascribe such a discrepancy to the absence of filler-matrix interactions in the derivation of Maxwell-Garnett formula. Enhancement on dielectric properties of nanocomposites due to interfacial polarizations has been reported previously.[4,10–14] In this work, HEMA containing polar —OH functional groups was adopted as the coupling agent of organic and inorganic phases. This may result in interfacial polarization due to its presence at the organic/inorganic interfaces as illustrated in Figure 8. As the inorganic filler loading increases, more organic/inorganic interfaces are generated in the nanocomposites, and hence escalate the interfacial polarizations. In conjunction with the addition of high-dielectric nano-scale Ta_2O_5 filler, the dielectric constant enhancement of nanocomposites was hence observed.

During the sample preparation, poly-HEMA derived from HEMA monomer and poly-TMMA derived form MMA and TMPTA monomers might also form in the nanocompiste samples. Because they are randomly distributed in polymeric matrix, the contribution of poly-HEMA and poly-TMMA to the dielectric constant enhancement can thus be evaluated by using the mixture rule as follows[9,37]:

$$\varepsilon_{com} = \varepsilon_1 x + \varepsilon_2(1 - x) \quad (5)$$

where ε_{com} is dielectric constant of composite, ε_1 is dielectric constant of Component 1, ε_2 is dielectric constant of Component 2, and x is the volume fraction of Component 1. It was measured that the dielectric constants of PHEMA and PTMMA are about 3.52 and 2.37 (at 1 MHz), respectively. The calculation shows that the dielectric constant is about 2.6 for pristine polymer derived from HEMA, MMA, and TMPTA monomers, which is very close to the experimental value 2.53. This indicates that the addition of HEMA barely affects the dielectric constant

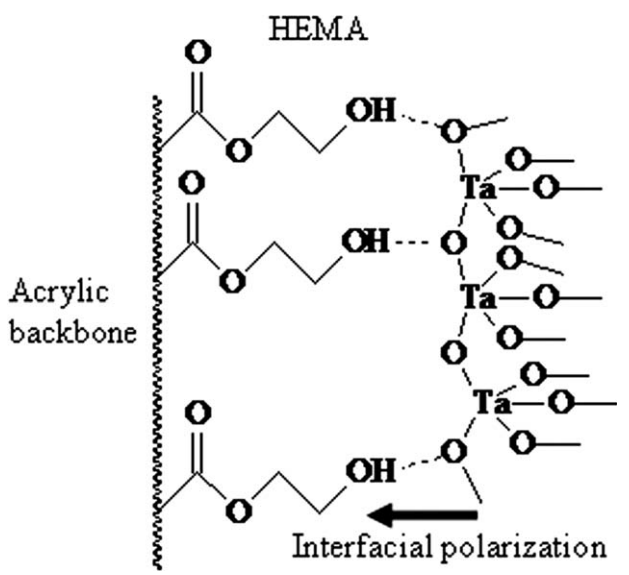

Figure 8 Schematic illustration of the interfacial polarization at Ta_2O_5/acrylic interface.

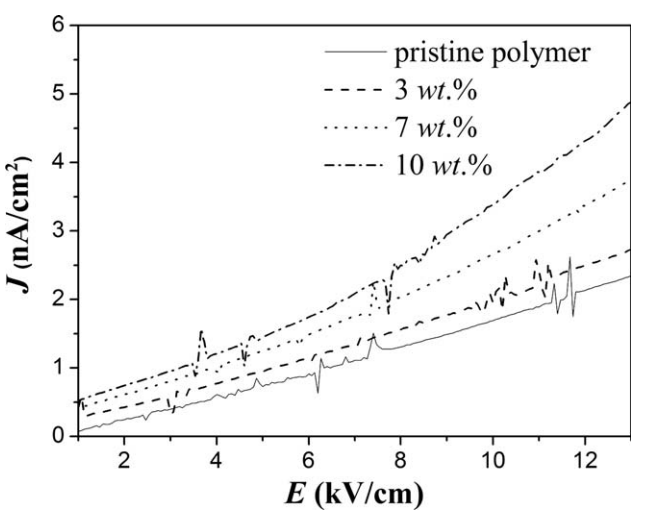

Figure 9 *J-E* profiles for pristine polymer and nanocomposite samples.

property of pristine polymer. As to the nanocomposite samples, they contain the same amount of HEMA as in pristine polymer and HEMA serves as the coupling agent of organic and inorganic phases. Its contribution to dielectric constant enhancement is amplified with the increase of specific surface area (SSA) when the inorganic filler size becomes nanoscale.

Figure 9 shows the leakage current density (J) versus applied bias field (E) for pristine polymer and nanocomposite samples. In addition to the absence of electrical breakdown, the leakage current density of the nanocomposites is lower than 5.5 nA/cm^2 in the range of applied field up to 13 kV/cm. Although the leakage current increase with the Ta_2O_5 filler loading, such a low leakage current density indicates the addition of Ta_2O_5 nanoparticles does not dramatically promote the charge carrier migration in the acrylic matrix. Furthermore, the J-E curves for all samples exhibit the linear ohmic behavior of at low applied field as shown in Figure 9. At high applied field, the nanocomposites with high filler contents possess a higher increasing trend of leakage current density. This is attributed to the charge carrier trapping sites generated by the implantation of inorganic filler. They allow the charge carrier transport, and thus raise the leakage current in the samples.[38]

CONCLUSIONS

Ta_2O_5 nanoparticles were synthesized by a chemical route using OLEA as the surfactant and solvent to confine the Ta_2O_5 growth so as to yield the nanoscale oxide particles. The scaled down of particle size was found to effectively suppress the recrystallization temperature of Ta_2O_5 that the orthorhombic phase could be obtained by annealing at a temperature below 750°C, an at least 50°C suppression in comparison with that of bulk Ta_2O_5. The UV-curable Ta_2O_5-acrylic nanocomposite samples were prepared accordingly and the TEM characterization revealed that the dispersion of Ta_2O_5 nanoparticles in polymer matrix can be achieved via the addition of HEMA coupling agent incorporating with mechanical agitation. Substantial improvements on thermal stability and dielectric properties were observed due to the incorporation of Ta_2O_5 fillers in acrylic polymer. The relative dielectric constants of nanocomposites were found to increase from 2.53 to 4.23 (at 1 MHz) with the increase of filler loading up to 10 wt % of Ta_2O_5 without severe deterioration of dielectric loss. The improvement on dielectric properties was ascribed to the incorporation of high-dielectric nano-scale inorganic fillers in the samples and the presence of interfacial polarization resulted from the interactions at the organic/inorganic interface. Analytical results also indicated a limitation of filler loading in the UV-curable nanocomposites that excessive filler amount might cause prolonged UV curing and result in the photo-degradation of polymeric component. A careful control on filler loading is thus essential for the preparation of photo-curable nanocomposites with desired physical/chemical properties.

References

1. Katz, H. E. Chem Mater 2004, 16, 4748.
2. Forrest, S. R. Nature 2004, 428, 911.
3. Hong, J. I.; Winberg, P.; Schadler, L. S. Mater Lett 2005, 59, 473.
4. Cho, S. D.; Lee, J. Y.; Hyun, J. G.; Paik, K. W. Mater Sci Eng B 2004, 110, 233.
5. Yang, T. I.; Kofinas, P. Polymer 2007, 48, 791.
6. Maliakal, A.; Katz, H.; Cotts, P. M.; Subramoney, S.; Mirau, P. J Am Chem Soc 2005, 127, 14655.
7. Sihvola, A. Electromagnetic Mixing Formulas and Applications; The Institution of Electrical Engineers: London, 1999.
8. Todd, M. G.; Shi, F. G. J Appl Phys 2003, 94, 4551.
9. Su, W. F.; Lee, J. F.; Chen, M. Y.; Ho, R. M. J Mater Res 2004, 19, 2343.
10. Vo, H. T.; Shi, F. G. Microelectronics J 2002, 33, 409.
11. Murugaraj, P.; Mainwaring, D.; Mora-Huertas, N. J Appl Phys 2005, 98, 054304.
12. Dang, Z. M.; Xu, H. P.; Wang, H. Y. Appl Phys Lett 2007, 90, 012901.
13. Dang, Z. M.; Xie, D.; Shi, C. Y. Appl Phys Lett 2007, 91, 222902.
14. Deepa, K. S.; Sebastian, M. T.; James, J. Appl Phys Lett 2007, 91, 202904.
15. Qi, L.; Lee, B. I.; Chen, S.; Samuels, W. D.; Exarhos, G. J. Adv Mater 2005, 17, 1777.
16. Jiang, M. J.; Dang, Z. M.; Xu, H. P. Appl Phys Lett 2007, 90, 42914.
17. Dang, Z. M.; Lin, Y. H.; Nan, C. W. Adv Mater 2003, 15, 1625.
18. Xu, J.; Wong, C. P. Appl Phys Lett 2005, 87, 082907.
19. Lide, D. R. CRC Handbook of Chemistry and Physics, 84th ed.; CRC Press: Boca Raton, FL, 2003–2004.
20. Bartic, C.; Jansen, H.; Campitelli, A.; Borghs, S. Org Electron 2002, 3, 65.
21. Cozzoli, P. D.; Kornowski, A.; Weller, H. J Am Chem Soc 2003, 125, 14539.
22. Wang, X.; Zhuang, J.; Peng, Q.; Li, Y. Nature 2005, 437, 121.
23. Brinker, C. J.; Scherer, G. W. Sol-Gel Science: The Physics and Chemistry of Sol-Gel Processing; Academic Press: London, 1990.
24. Atanassova, E.; Spassov, D. Appl Surf Sci 1998, 135, 71.
25. Cullity, B. D.; Stock, S. R. Elements of X-Ray Diffraction, 3rd ed.; Prentice Hall: Upper Saddle River, NJ, 2001.
26. Gonzalez, J.; Ruiz, M. D. C.; Rivarola, J. B.; Pasquevich, D. J Mater Sci 1998, 33, 173.
27. Jooste, R.; Viljoen, H. J. J Mater Res 1998, 13, 475.
28. Masse, J. P.; Szymanowski, H.; Zabeida, O.; Amassian, A.; Klemberg-Sapieha, J. E.; Martinu, L. Thin Solid Films 2006, 515, 1674.
29. Hung, C. H.; Huang, W. T. J Mater Chem 2005, 15, 267.
30. Hamid, S. H.; Amin, M. B.; Maadhah, A. G. Handbook of Polymer Degradation; Marcel Dekker, Inc.: New York, 1992.
31. Wang, Y. Y.; Hsieh, T. E. Macromol Chem Phys 2007, 208, 2396.
32. Kaczmarek, H.; Chaberska, H. Appl Surf Sci 2006, 252, 8185.
33. Little, E. A. Phys Rev 1955, 98, 978.
34. Xu, F.; Trolier-McKinstry, S.; Ren, W.; Xu, B.; Xie, Z. L.; Hemker, K. J. J Appl Phys 2001, 89, 1336.
35. Ying, K. L.; Hsieh, T. E. Mater Sci Eng B 2007, 138, 241.
36. Ying, K. L.; Hsieh, T. E. Jpn J Appl Phys 2008, 47, 1947.
37. Petrovsky, V.; Manohar, A.; Dogan, F. J Appl Phys 2006, 100, 014102.
38. Hong, J. K.; Kim, H. R.; Park, H. H. Thin Solid Films 1998, 332, 449.